On the motion of unsteady translating bubbles in an unbounded Hele-Shaw cell

A. H. Khalid, N. R. McDonald, and J.-M. Vanden-Broeck

Citation: Physics of Fluids (1994-present) **27**, 012102 (2015); doi: 10.1063/1.4905582
View online: http://dx.doi.org/10.1063/1.4905582
View Table of Contents: http://scitation.aip.org/content/aip/journal/pof2/27/1?ver=pdfcov
Published by the AIP Publishing

PHYSICS OF FLUIDS **27**, 012102 (2015)

On the motion of unsteady translating bubbles in an unbounded Hele-Shaw cell

A. H. Khalid,[a] N. R. McDonald, and J.-M. Vanden-Broeck
Department of Mathematics, University College London, Gower Street, London, WC1E 6BT, United Kingdom

(Received 1 August 2014; accepted 13 December 2014; published online 13 January 2015)

Unsteady propagating bubbles in an unbounded Hele-Shaw cell are considered numerically in the case of zero surface tension. The instability of elliptical bubbles and their evolution toward a stable circular boundary, with speed twice that of the fluid speed at infinity, is studied numerically and by stability analysis. Numerical simulations of bubbles demonstrate that the important role played by singularities of the Schwarz function of the bubble boundary in determining the evolution of the bubble. When the singularity lies close to the initial bubble, two types of topological change are observed: (i) bubble splitting into multiple bubbles and (ii) a finite fluid blob pinching off inside the bubble region. © *2015 AIP Publishing LLC.* [http://dx.doi.org/10.1063/1.4905582]

I. INTRODUCTION

Hele-Shaw flows describe the motion of a viscous fluid sandwiched in a thin gap between two parallel plates. Since the equations of Hele-Shaw flows are analogous to the equations of two dimensional (2D) flow in porous media, the solutions and dynamics of free boundary problems in Hele-Shaw flows have attracted a great deal of interest. Moreover, Hele-Shaw free boundary flows have revealed unexpected connections to other fields of mathematics and its applications, for example, integrable systems[1,2] and random matrices.[3]

The evolution of the free boundary separating viscous fluid from a region of inviscid fluid (i.e., a bubble) has been an active area of research interest due to physical applications such as oil extraction, a study which gave rise to the Polubarinova-Galin equation,[4,5] where analytical solutions were found for a parametric complex variable polynomial map. The motion of travelling interfaces was considered by Taylor and Saffman[6,7] in the form of infinitely long travelling fingers constrained by a channel in a Hele-Shaw cell and travelling bubbles in a channel with a steady uniform background flow.[6–8] In both cases, mathematical analysis revealed a continuous family of possible solutions, each member occupying a different width of the channel. However, in experiments, the observed finger is half the channel width;[7] the selection of such can be calculated by introducing surface tension T and then taking the limit as T tends to zero.[8–10] More recently, the selection of particular solutions of the solution family has been proposed as a fundamental stability property of zero surface tension (ZST) Hele-Shaw flows.[11,12] That selection is determined entirely by the ZST dynamics has led to much debate in the literature.[10,13–17] Moreover, the ZST problem is ill-posed in the sense that small perturbations may cause large effects in the resulting interface evolution.[18,19] The present work uses numerical smoothing to regularise the problem enabling convergent numerical results to be computed. The choice to use smoothing rather than surface tension offers an alternative way to understand the selection problem for bubbles in an unbounded Hele-Shaw cell.

Bubble breakup and the associated change in topology has also been of interest in Hele-Shaw flows.[20–23] The breakup of a stream of bubbles rising in a Hele-Shaw cell have also been considered experimentally.[24] The simplest case of the breakup of a single bubble travelling in an unbounded

[a]ali.khalid@ucl.ac.uk

Hele-Shaw cell appears not to have been studied previously and is considered here for various initial bubble shapes in the case of ZST. It is shown that singularities of the Schwarz function of the initial interface play an important role in the evolution of the interface, in that the bubble "avoids" contact with the singular point.

Many regularised problems of Hele-Shaw flows, e.g., flows including effects such as surface tension or kinetic undercooling, have invited numerical solutions of the free boundary problem.[25–28] Many formulations of the numerical methods are based on boundary integral equations (BIEs) due to the simplicity of the underlying equations, where, for example, a spectrally accurate spatial discretisation can be employed.[28] In many cases, the boundary integral equations are formulated using Green's second identity and letting the point of observation approach the interface between the two fluids.[26] Another popular method used to formulate an integral equation on the free boundary is the vortex sheet method.[29,30] The approach taken in the present work is also to formulate as a boundary integral equation in the complex plane using Cauchy's integral formula.

This paper is organised as follows. The problem is formulated in Sec. II and a brief background on the Taylor-Saffman bubble in an unbounded cell is given. The numerical procedure is described in Sec. III. Numerical results are discussed in Sec. IV and a stability analysis of elliptical bubbles is presented in Sec. V, before ending with some concluding remarks in Sec. VI.

II. MATHEMATICAL MODEL

The motion of the interface $\partial\Omega(t)$ is determined by hydrodynamics with the fluid occupying an infinite domain $\Omega(t)$ punctured by a simply connected "air" bubble of constant pressure and boundary $\partial\Omega(t)$. In dimensionless form, we write the 2D velocity vector as $\mathbf{u} = \nabla\phi$. Considering conservation of mass, $\nabla \cdot \mathbf{u} = 0$, the governing equations for the resulting free boundary problem are

$$\nabla^2\phi = 0, \qquad (x, y) \in \Omega(t), \tag{1a}$$

$$\phi = 0, \qquad (x, y) \in \partial\Omega(t), \tag{1b}$$

$$v_n = \frac{\partial\phi}{\partial n}, \quad (x, y) \in \partial\Omega(t), \tag{1c}$$

where $\phi(x, y, t)$ is a real harmonic function in $\Omega(t)$, v_n is the normal velocity of $\partial\Omega(t)$, and $\mathbf{n}$ the outward pointing unit normal vector on $\partial\Omega(t)$ relative to the bubble region. Here, $\partial/\partial n$ denotes the derivative in the normal direction, i.e., $\partial/\partial n = \mathbf{n} \cdot \nabla$. For a bubble in the presence of a uniform steady background flow with speed V, the above problem is supplemented by the condition

$$\phi \to Vx, \quad \text{as } x, y \to \pm\infty, \tag{2}$$

i.e., without loss of generality, a uniform flow parallel to the x-axis. Therefore, due to the pressure gradient, the bubble translates downstream at speed $U(t)$ which needs to be determined along with the bubble shape $\partial\Omega(t)$. Equations (1b) and (1c) represent the dynamic and kinematic boundary conditions, respectively.

Setting $z = x + iy$, the free boundary problem described by (1) and (2) can be reformulated using complex variable methods and the Schwarz function, $\mathcal{S}(z, t)$, of the interface in order to find exact solutions. The Schwarz function is an analytic function in the neighbourhood of $\partial\Omega(t)$ such that $\overline{z} = \mathcal{S}(z, t)$ on $\partial\Omega(t)$, where the bar denotes complex conjugation. The governing equation derived from (1) given by

$$\frac{\partial w}{\partial z} = \frac{1}{2}\frac{\partial \mathcal{S}}{\partial t} \tag{3}$$

is known as the Schwarz function equation, where $w = \phi + i\psi$ is the complex potential of the flow and ψ the harmonic conjugate of ϕ (i.e., the stream function).[1,31]

Explicit solutions can be sometimes found by studying the singularity structure of (3) via a time dependent conformal map from an auxiliary ζ-plane to the physical z-plane. This gives an initial value problem in terms of the unknown time dependent parameters of the conformal map.[32,33] For simply connected domains describing bubbles in an unbounded Hele-Shaw cell, either the

interior or exterior of the unit ζ-disc can be mapped conformally on to the viscous fluid region by $z = f(\zeta,t)$, where the fluid interface is given by $|\zeta| = 1$. Hence, the Schwarz function of the interface is defined as $\mathcal{S} = \overline{z} = \overline{f}(1/\zeta,t)$, and (3) can be analytically continued away from the interface to hold over $\Omega(t)$. This idea has been used to derive explicit solutions, e.g., the evolution of fluid blobs due to hydrodynamic singularities[31] or even external fields[32] and is also used here to understand the evolution of bubbles.

A. The Taylor-Saffman bubble in an unbounded cell

Taylor and Saffman considered the now well-known problem of translating symmetric bubbles in a Hele-Shaw cell, in which the viscous fluid region is constrained by a parallel sided channel.[7] They found a family of solutions governed by the bubble speed and maximum bubble width. Previous to this, Saffman and Taylor considered the motion of an infinitely long bubble in the channel (the Saffman-Taylor finger), where the observed selected solution is half the width of the channel.[6]

Taylor and Saffman claim that in the case of a small bubble in a channel (or equivalently an unbounded cell),[7] surface tension effects are comparable with changes in fluid pressure near the bubble interface and it is the surface tension that makes the perimeter of the bubble as short as possible, therefore making the bubble circular, which necessarily travels at speed twice the background flow, i.e., $U = 2V$. Following the works of Taylor and Saffman,[6,7] many works have been carried out on the so called selection problem numerically, experimentally, and theoretically, some of which are cited here[8,9,11,12,34] (see also references therein).

An alternative theory in which surface tension plays no role in the selection mechanism of a finger of half the channel width has been proposed by Mineev-Weinstein.[11] Mineev-Weinstein uses stability analysis to show that the half-width finger is the only attractor for time-dependent solutions which remain non-singular for all time.

The above result has recently been extended to finite bubbles travelling in a channel,[12] where it is shown that the bubble with $U = 2V$ is selected as it is a fixed point attractor of the ZST translating bubble problem. In an unbounded Hele-Shaw cell, or small bubble limit in a channel geometry, this corresponds to the circular bubble. In this paper, the ZST problem for unsteady bubbles in an unbounded cell is studied numerically. The selection problem is considered as well as cases of bubble breakup.

B. The elliptical bubble: A steady shape solution to the Hele-Shaw free boundary problem

The elliptical bubble is a steady solution of the Hele-Shaw free boundary problem in an unbounded cell and so is any rotation of the ellipse due to the rotation invariance of steady Hele-Shaw flows.[35] That is, the map given by

$$z(\zeta,t) = C + e^{i\theta_e}\left(a\zeta + \frac{b}{\zeta}\right) \tag{4}$$

is a solution to the Hele-Shaw problem, where the time-varying parameters a, b, and θ_e are real such that $b \neq 0$, and in general, C is complex valued. Here, (4) represents a conformal map from the interior of the unit ζ-disc, $D = \{\zeta : |\zeta| \leq 1\}$, to the exterior of the bubble, i.e., the flow domain $\Omega(t)$. The interface $\partial\Omega(t)$ is mapped from $\partial D = \{\zeta : |\zeta| = 1\}$. The speed of the bubble can be found using the Schwarz function approach as follows. First, considering map (4), the Schwarz function of $\partial\Omega(t)$ is given by

$$\mathcal{S}(\zeta,t) = \overline{z}(1/\zeta,t) = \overline{C} + e^{-i\theta_e}\left(\frac{a}{\zeta} + b\zeta\right). \tag{5}$$

As $\zeta = 0$ maps to infinity, from (4) we see that as $z \to \infty$

$$\zeta = \frac{be^{i\theta_e}}{z - C} + O((z - C)^{-3}), \tag{6}$$

and thus the time derivative of the Schwarz function in (5) as $z \to \infty$ is given by

$$\frac{\partial \mathcal{S}}{\partial t}(z,t) = \frac{d\overline{C}}{dt} + \frac{a}{b}(z-C)\frac{d}{dt}(e^{-2i\theta_e}) + e^{-2i\theta_e}\frac{d}{dt}\left(\frac{a}{b}(z-C)\right) + O((z-C)^{-1}). \tag{7}$$

If the background flow is given by a uniform flow of speed V, then as $z \to \infty$, the complex potential takes the form $w = Vz$. Since the Schwarz function Eq. (3) must hold over $\Omega(t)$, from (7), as $z \to \infty$ at $O(1)$ and $O(z)$

$$\frac{d}{dt}\left(\overline{C} - e^{-2i\theta_e}\frac{a}{b}C\right) = 2V, \tag{8a}$$

$$\frac{d}{dt}\left(e^{-2i\theta_e}\frac{a}{b}\right) = 0. \tag{8b}$$

In addition to (8a) and (8b), the bubble area, A, must also be conserved where

$$A = \left|\frac{1}{2i}\oint_{\partial D}\overline{z}z_\zeta d\zeta\right| = \pi\left|a^2 - b^2\right| \tag{9}$$

is calculated using the complex form of Green's theorem. That is, $|a^2 - b^2| = A/\pi$ is constant and together with (8b) implies that a, b, and θ_e are constant. Employing (8b) in (8a) and taking the real and imaginary parts gives

$$\dot{C}_R - \frac{a}{b}\left(\dot{C}_R\cos(2\theta_e) + \dot{C}_I\sin(2\theta_e)\right) = 2V, \tag{10a}$$

$$-\dot{C}_I - \frac{a}{b}\left(\dot{C}_I\cos(2\theta_e) - \dot{C}_R\sin(2\theta_e)\right) = 0, \tag{10b}$$

where C_R and C_I denote the real and imaginary parts of $C(t)$, respectively. Here, the dot denotes derivative with respect to time. Solving (10) for $\dot{C}_R$ and $\dot{C}_I$, and integrating, gives

$$C(t) = \frac{2Vt}{1 - a^2/b^2}\left(1 + \frac{a}{b}\cos(2\theta_e) + i\frac{a}{b}\sin(2\theta_e)\right), \tag{11}$$

where $U = \dot{C}$ gives the bubble velocity. That is, the angle at which the bubble propagates steadily with respect to $\Re(z)$ is given by $\tan^{-1}(((a/b)\sin(2\theta_e))/(1 + (a/b)\cos(2\theta_e)))$, which agrees with the result given by Tian and Vasconcelos.[35] Note that for a circular bubble $a = 0$ and from (10a) and (10b) $U = 2V$, i.e., the bubble propagates in the purely real direction with twice the background flow speed. The stability of the steady shape elliptical solutions is tested numerically in Sec. IV A.

III. NUMERICAL MODEL

The velocity potential of the flow is decomposed as $\phi = \widetilde{\phi} + \widehat{\phi}$ where the velocity potential due to the given background flow is $\widehat{\phi}(z,\overline{z},t)$, and $\widetilde{\phi}(z,\overline{z},t)$ is the potential part due to the presence of the bubble. The velocity $\widetilde{\mathbf{u}} = \nabla\widetilde{\phi}$ is a solenoidal, irrotational vector field which describes the local evolution of the bubble interface as a result of the background flow, $\widehat{\mathbf{u}} = \nabla\widehat{\phi}$. The total fluid velocity is given by the sum $\mathbf{u} = \widetilde{\mathbf{u}} + \widehat{\mathbf{u}}$. In order to solve (1), the free boundary problem is written in terms of $\widetilde{\phi}$, i.e.,

$$\nabla^2\widetilde{\phi} = 0, \qquad z \in \Omega(t), \tag{12a}$$

$$\widetilde{\phi} = -\widehat{\phi}, \qquad z \in \partial\Omega(t), \tag{12b}$$

$$v_n = \frac{\partial}{\partial n}\left(\widetilde{\phi} + \widehat{\phi}\right), \quad z \in \partial\Omega(t), \tag{12c}$$

where $\widehat{\phi} = Vx = V(z + \overline{z})/2$ and

$$\widetilde{\phi} \to 0, \quad \text{as } z \to \infty. \tag{13}$$

The numerical method is to first solve (12a) and (12b) to find $\widetilde{v}_n$ at any instance given $\Omega(t)$ and then to advect the interface by kinematic condition (12c). Explicit time notation is suppressed for brevity in what follows.

A. Mathematical formulation

Equations (12a) and (12b) can be formulated as a BIE by considering the Cauchy transform of the complex velocity potential $\widetilde{w}'(z) = \widetilde{u}(z) - i\widetilde{v}(z)$ for $z \in \partial\Omega$. Here, prime denotes derivative with respect to z. The formulation and algorithm follows previous work[33] with some modifications, which are derived here for completeness. Since $\widetilde{w}'(z)$ is an analytic function for all z in the fluid domain, Ω, considering the Cauchy transform and applying the Cauchy integral formula yields

$$\frac{1}{2i\pi}\int_{\partial\Omega}\frac{\widetilde{u}(z)-i\widetilde{v}(z)}{z-z_m}\,dz = -\frac{1}{2}\left(\widetilde{u}(z_m)-i\widetilde{v}(z_m)\right), \quad z_m \in \partial\Omega. \tag{14}$$

Here, $\partial\Omega$ describes a simple closed contour in the complex plane. The parameterisation is such that the contour is traversed in the anticlockwise direction and the minus sign on the right hand side of (14) accounts for the viscous fluid region lying on the exterior (to the right) of $\partial\Omega$. Parameterising the interface with the arc length, s, i.e., $z(s) = x(s) + iy(s)$ where $x_s^2 + y_s^2 = 1$ (the subscript s denoting differentiation with respect to s) and taking the unit normal, $\mathbf{n}(s)$ on $\partial\Omega$, pointing into Ω, then

$$(\widetilde{u}(s) - i\widetilde{v}(s))\frac{dz}{ds} = \widetilde{v}_\tau(s) + i\widetilde{v}_n(s), \quad z(s) \in \partial\Omega, \tag{15}$$

where $\widetilde{v}_\tau$ and $\widetilde{v}_n$ denote the tangential and normal velocity of a fluid particle on the interface. The normal and tangential vectors ($\mathbf{n}$ and $\boldsymbol{\tau}$) on the interface are defined as $(y_s, -x_s)$ and (x_s, y_s), respectively. Differentiating (12b) along the interface gives the boundary condition in terms of tangential velocity $\widetilde{v}_\tau$, i.e.,

$$\widetilde{v}_\tau(z) = -\widehat{v}_\tau(z) = -\frac{\partial}{\partial\tau}(Vx), \quad z \in \partial\Omega, \tag{16}$$

and so $\widetilde{v}_\tau$ is known on $\partial\Omega$. Using (15) and (16) allows (14) to be written in terms of the unknown normal velocity $\widetilde{v}_n$, i.e.,

$$\int_0^L \frac{-\widehat{v}_\tau(s) + i\widetilde{v}_n(s)}{z(s) - z(s_m)}\,ds = -i\pi\left(-\widehat{v}_\tau(s_m) + i\widetilde{v}_n(s_m)\right)\left(\frac{dz}{ds}(s_m)\right)^{-1}, \tag{17}$$

where L denotes the total arc length of the contour $\partial\Omega$ and the integral on the left hand side is a Cauchy principle value integral.

Equation (17) satisfies (12a) and (12b), hence, one can solve the real part of (17) for $\widetilde{v}_n$ from which the total fluid velocity $\mathbf{u} = \widetilde{\mathbf{u}} + \widehat{\mathbf{u}}$ can be constructed on $\partial\Omega$. When the fluid velocity is found, the interface is advected according to (12c), i.e.,

$$\frac{d\mathbf{x}}{dt} = \mathbf{u}. \tag{18}$$

B. Numerical procedure

At time $t = t_j$, the numerical solution to BIE (17) is considered when the interface $\partial\Omega$ has total arc length L. All quantities are taken at time t_j unless stated otherwise. On the interval $[0, L]$, $N + 1$ equispaced mesh points are constructed such that

$$S_1 = 0, \tag{19a}$$

$$S_{i+1} = S_i + \Delta S, \quad i =, 1 \ldots, N, \tag{19b}$$

where the mesh size is given by

$$\Delta S = \frac{L}{N} = \frac{S_{N+1}}{N}, \tag{20}$$

and N midpoints are defined as

$$S_{i+\frac{1}{2}} = S_i + \frac{\Delta S}{2}. \tag{21}$$

Equation (17) is re-arranged in the form

$$\int_0^L \frac{i\widetilde{v}_n(s)}{z(s)-z(s_m)}\,ds - \pi\widetilde{v}_n(s_m)\left(\frac{dz}{ds}(s_m)\right)^{-1} = g(z(s_m)), \tag{22}$$

where $g(z(s_m))$ is a known function given by

$$g(z(s_m)) = \int_0^L \frac{\widehat{v}_\tau(s)}{z(s)-z(s_m)}\,ds + i\pi\widehat{v}_\tau(s_m)\left(\frac{dz}{ds}(s_m)\right)^{-1}, \tag{23}$$

and s_m is chosen to coincide with $S_{m+\frac{1}{2}}$.

New variables for the discretisation of $\partial\Omega$ are defined as

$$Z_i = z(S_i), \quad i = 1,\ldots,N+1, \tag{24}$$

and the unknown quantities to be found are

$$\alpha_i = \widetilde{v}_n(S_i), \quad i = 1,\ldots,N+1. \tag{25}$$

The periodic conditions $Z_{N+1} = Z_1$ and $\alpha_{N+1} = \alpha_1$ hold since $\partial\Omega$ is assumed to be a simple closed contour at each time step. Let the right hand side of (22) be $G_m = g(Z_{m+\frac{1}{2}})$. The quantity $\widetilde{v}_n(s_m) = \widetilde{v}_n(S_{m+\frac{1}{2}}) = \alpha_{m+\frac{1}{2}}$ is approximated linearly between neighbouring points, i.e.,

$$\alpha_{m+\frac{1}{2}} = \frac{1}{Z_{m+1}-Z_m}\left[\left(Z_{m+1}-Z_{m+\frac{1}{2}}\right)\alpha_m + \left(Z_{m+\frac{1}{2}}-Z_m\right)\alpha_{m+1}\right]. \tag{26}$$

The integrals in (22) are approximated using the trapezium rule. Since the singular points s_m are taken to coincide with the midpoints of the mesh, $S_{m+\frac{1}{2}}$, the integral is evaluated by ignoring the singularities with an accuracy no less than that of a non-singular integral.[36,37] Taking into account the periodicity on the interface, the integral in discrete form is approximated as

$$\int_0^L \frac{i\widetilde{v}_n(s)}{z(s)-z(s_m)}\,ds \approx \sum_{j=1}^{N}\frac{i\alpha_j}{Z_j - Z_{m+\frac{1}{2}}}\Delta S, \quad m = 1,\ldots,N. \tag{27}$$

The derivatives in (22), i.e., $z_s(s_m)$, are approximated via a fourth order centred finite difference formula. Thus, employing (26) and (27) in (22), and taking the real part, gives a system of N linear equations for the unknown α_i, for $i = 1,\ldots,N$, which can be written in matrix form as

$$\mathbf{M}\boldsymbol{\alpha} = \mathbf{G}. \tag{28}$$

Matrix equation (28) is solved giving the normal velocity (the vector $\boldsymbol{\alpha}$) of fluid particles on $\partial\Omega$ coinciding with the mesh at time $t = t_j$.

Since in the case of translating bubbles, the area of the bubble is conserved in time, the solution $\boldsymbol{\alpha}$ is purged at each time step following the method given by Kelly and Hinch,[26] where we set

$$\alpha_i = \alpha_i - \left(\oint_{\partial\Omega}\widetilde{v}_n(s)\,ds\right)\left(\oint_{\partial\Omega}ds\right)^{-1} \approx \alpha_i - \frac{1}{L}\sum_{i=1}^{N}\alpha_i, \quad i = 1,\ldots,N, \tag{29}$$

ensuring the total fluid flux across $\partial\Omega$ due to the velocity field $\widetilde{\mathbf{u}}$ is zero. Largely, the use of (29) had little effect since the solution to (28) conserved mass to a good approximation.

It remains to compute the evolution of $\partial\Omega$ in time given the vector $\boldsymbol{\alpha}$. The evolution can be approximated at the following time step $t_{j+1} = t_j + \Delta t$ as

$$\begin{aligned} z(S_i(t_j+\Delta t), t_j+\Delta t) &\approx z(S_i,t_j) + \Delta t\left[\frac{\partial z}{\partial s}(S_i,t_j)\frac{dS_i}{dt} + \frac{\partial z}{\partial t}(S_i,t_j)\right] \\ &= z(S_i,t_j) + \Delta t\,\dot{z}(S_i,t_j), \end{aligned} \tag{30}$$

where $\dot{z}$ is the complex velocity of the interface. Since (12c) must be satisfied, and the interface evolves according to its normal velocity, the interface velocity is reconstructed from the total fluid velocity $\mathbf{u}(S_i,t) = \widetilde{\mathbf{u}}(S_i,t) + \widehat{\mathbf{u}}(S_i,t)$. The mesh points $Z_i = z(S_i,t) \in \partial\Omega$ can be treated as Lagrangian

particles and (30) is written in the form

$$\Re(Z_i^{\text{new}}) = \Re(Z_i) + u(S_i,t_j)\Delta t, \quad i = 1,\ldots,N, \tag{31}$$

$$\Im(Z_i^{\text{new}}) = \Im(Z_i) + v(S_i,t_j)\Delta t, \quad i = 1,\ldots,N, \tag{32}$$

where $Z_i^{\text{new}} \in \partial\Omega^{\text{new}}$, and $\partial\Omega^{\text{new}}$ is the new position of the interface $\partial\Omega$ at $t = t_j + \Delta t$. A modified Euler (i.e., a second order Runge-Kutta) method is employed, as by Baker,[37] such that the time stepping method is approximately $O((\Delta t)^2)$ accurate.

Once $\partial\Omega^{\text{new}}$ is found, the new total arc length L^{new} is computed from the mesh points Z_i^{new}, $i = 1,\ldots,N+1$, which are then redistributed to an equispaced mesh by cubic spline interpolation. Setting $Z_i = Z_i^{\text{new}}$ (i.e., $\partial\Omega = \partial\Omega^{\text{new}}$, $L = L^{\text{new}}$) and applying the above procedure again completes the algorithm for computing the interface at later times. Since the time stepping procedure is explicit in time, a stability constraint applies[30] in the form $\Delta t \le c(\Delta S)^n$ for some positive number n.

C. Numerical instabilities

The numerical method gives rise to "spurious oscillations" similar to those reported in other BIE methods,[30,38–40] and these errors may grow in time as the interface evolves.[39]

Aitchison and Howison[39] note the introduction of small wavelength instabilities into the solution of the numerical problem is a result of rounding errors and approximate solution techniques and shows that the frequency of the error oscillations scale with N. The difficulty being the more mesh points that are included (i.e., increasing N) shorter wavelength errors are permitted, and it is these which grow fastest in time.[6,39] To eliminate oscillatory errors, the solution requires filtering. In the current algorithm, filtering is carried out at each time step by solving a modified matrix equation which gives a sufficiently smooth solution as required by the physical problem. Specifically, (28) is modified to[41,42]

$$(\mathbf{M}^\top\mathbf{M} + \gamma\mathbf{H})\boldsymbol{\alpha} = \mathbf{M}^\top\mathbf{G}. \tag{33}$$

Here, $\mathbf{H}$ is the matrix representation of a third order difference operator[42] and γ denotes the smoothing parameter, where $0 < \gamma < \infty$ such that (33) gives a sufficiently accurate solution compared with an otherwise oscillatory solution from (28). Usually, increasing values of γ increases the smoothing effect on the solution. The filtering technique employed here is analogous to that of spectral methods,[30] for example, where the Fourier series is truncated and modes for the high frequency, small amplitude oscillations are neglected.

D. Numerical tests

The numerical method outlined above was tested against some exact, known solutions of the Hele-Shaw flow problem. These include the growth of finite fluid blobs by hydrodynamic singularities, e.g., sources or sinks (where the background flow potential $\widehat{\phi}$ is modified appropriately), and for flows driven by external background fields.[33] The numerical results give excellent agreement with the exact solutions. Furthermore, in the unstable regime, e.g., when the interface (given by a polynomial map) of a fluid blob is driven by a sink, the numerical solutions agree with exact solutions before cusp formation. In all the numerical results presented here, the smoothing parameter $\gamma = 1$ gives sufficiently smooth and accurate results. Also, the results are independent of this choice of γ, i.e., doubling or halving of γ leaves the numerical results essentially unchanged.

The numerical method is tested against the exact solution for a translating circular bubble in a uniform flow given in (11). In the case of a circular bubble, $a = 0$ and $U = 2V$. The background flow is given by (12c), i.e., $\widehat{\mathbf{u}} = (V,0)$. The exact normal velocity on the interface is $\mathbf{u}\cdot\mathbf{n} = (u,v)\cdot(y_s,-x_s)$, where the circular interface is parametrised with arc length, traversed in the anticlockwise direction. Subtracting the velocity due to the background flow on the interface gives the exact solution for the normal velocity due to the bubble, i.e.,

$$\begin{aligned}\widetilde{V}_n &= (\mathbf{u}-\widehat{\mathbf{u}})\cdot\mathbf{n}\\ &= ((2V,0)-(V,0))\cdot(y_s,-x_s)\\ &= V\,y_s\\ &= V\cos\Theta,\end{aligned} \tag{34}$$

where $s \equiv \Theta$ for a circular bubble of unit radius. The numerical solution of (22) is denoted by $\widetilde{v}_n$. Fig. 1 shows the convergence of the solution $\widetilde{v}_n$ towards the exact solution $\widetilde{V}_n$, as the number of mesh points N is increased, over one time step. The root mean square error (RMSE) is given by

$$\frac{1}{N}\left(\sqrt{\sum_{i}^{N}\left[\widetilde{v}_n(S_i)-\widetilde{V}_n(S_i)\right]^2}\right). \tag{35}$$

Here, the background flow speed is set to be $V = 1$. As expected, the errors decrease approximately as $O(1/N^3)$, as measured by the RMSE. This is because the largest errors occur in approximating the integral in (22) by the trapezium rule.

The effect of filtering on the numerical solution is presented in Fig. 2, where the solution $\widetilde{v}_n$ is given as a function of the angle $\Theta = \arg(z(s))$ for a circular bubble translating in a uniform flow. In the absence of filtering, the errors in approximating the right hand side of (22) give oscillatory solution about the corresponding smooth solution. When the filter is applied (by choosing a finite, non-zero value of γ), the smooth solution gives excellent agreement with the expected solution, in this case given by $\widetilde{V}_n = V\,y_s = \cos(\Theta)$.

IV. BUBBLES IN A HELE-SHAW CELL: NUMERICAL RESULTS

A. Attraction of elliptical bubbles to a circular bubble

Consider initial elliptical bubbles given by conformal map (4) from D, in the ζ-plane, to the exterior of the bubble, $\Omega(0)$, in the z-plane, in an unbounded Hele-Shaw cell. The time evolution of the interface produced by the numerical results is given in Fig. 3 for three values of θ_e, all with same

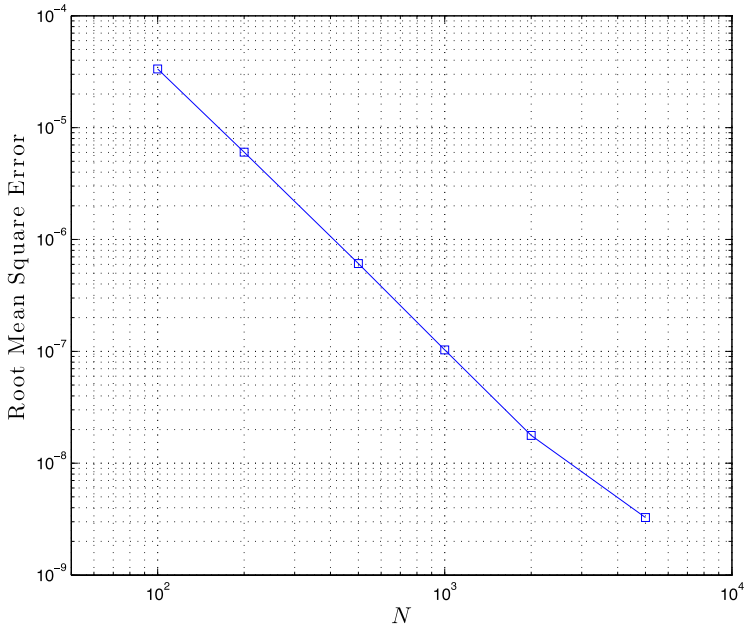

FIG. 1. The decrease in RMSE of the normal velocity of a circular bubble of unit radius as the number of mesh points is increased from $N = 100$ to $N = 5000$. In all tests, the algorithm is run for one fixed time step $\Delta t = 0.001$.

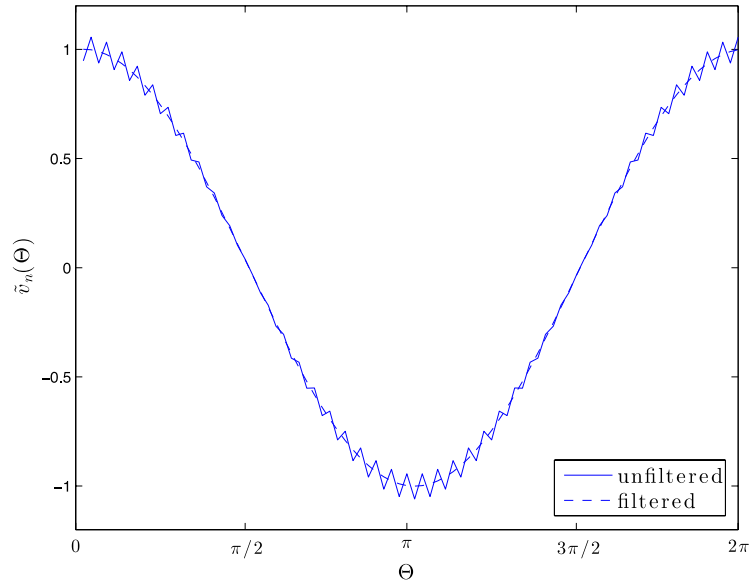

FIG. 2. Oscillations of (unfiltered) numerical solution $\widetilde{v}_n$ after one time step with $N = 140$ and $\Delta t = 0.001$, superimposed on the smooth (filtered) solution where the smoothing parameter is $\gamma = 0$ (unfiltered) and $\gamma = 1$ (filtered), respectively. The solution presented corresponds to a circular bubble of unit radius in a uniform background flow with $V = 1$.

area and aspect ratio. In all cases, the bubble evolves rapidly (within a distance of 2–3 major axis lengths) to the circular solution and then translates steadily with speed $U = 2V$.

The velocity of the centre of mass of the bubble can be calculated given the normal velocity on the interface by [43]

$$\dot{z}_{cm} = \frac{1}{A}\int_0^L z\mathbf{u}.\mathbf{n}\, ds, \tag{36}$$

where $\dot{z}_{cm}$ denotes the velocity of the centre of mass in complex form. The speed of the centre of mass can thus be calculated as $v_{cm} = |\dot{z}_{cm}|$. The velocity in (36) is computed numerically at each time step. The real and imaginary (i.e., x and y) components of $\dot{z}_{cm}$, and the speed of the centre of mass v_{cm} is plotted as functions of time in Fig. 4. As expected, elliptical bubbles with semi-major axis aligned in the direction of the background flow ($\theta_e = 0$) decelerate to the steady solution $U = 2V$ as they become circular. It was noted by Taylor and Saffman[7] that bubbles elongated in the direction of the flow travel with increased speed, i.e., greater than $2V$. Elliptical bubbles with semi-major axis perpendicular to the background flow accelerate (cf. Fig. 4, $\theta_e = \pi/2$) to $U = 2V$ while becoming circular.

If $0 < \theta_e < \pi/2$, then the bubble interface adjusts to the steady circular solution as $\Im(\dot{z}_{cm}) \to 0$. Therefore, starting with initially elliptical interface with arbitrary inclination to the uniform background flow, the bubble evolves to the steady circular solution as $t \to \infty$ travelling with speed $U = 2V$, parallel to the background flow—see curves in Fig. 4 with $\theta_e = \pi/4$.

It is interesting to note that for a short time after $t = 0$, the bubble speed adjusts only slowly as the interface remains approximately elliptical before instability sets in. Figs. 5(a) and 5(b) show a close-up of the evolution of $v_{cm}(t)$ for small time and corresponding snapshots of the interface, respectively. This delay before instability is possibly a numerical effect and is now investigated.

Fig. 6 shows dependence of bubble speed for various values of mesh points, N. When N is increased (time step Δt remaining fixed), the solution approaches the circular solution more rapidly. This may seem counter-intuitive, however Aitchison and Howison[39] speculate that increasing N introduces shorter wavelength instabilities which grow the fastest, thus increasing resolution leads to a more rapid growth in instability. This result holds true for increasing N with $\Delta t/\Delta S$ fixed.

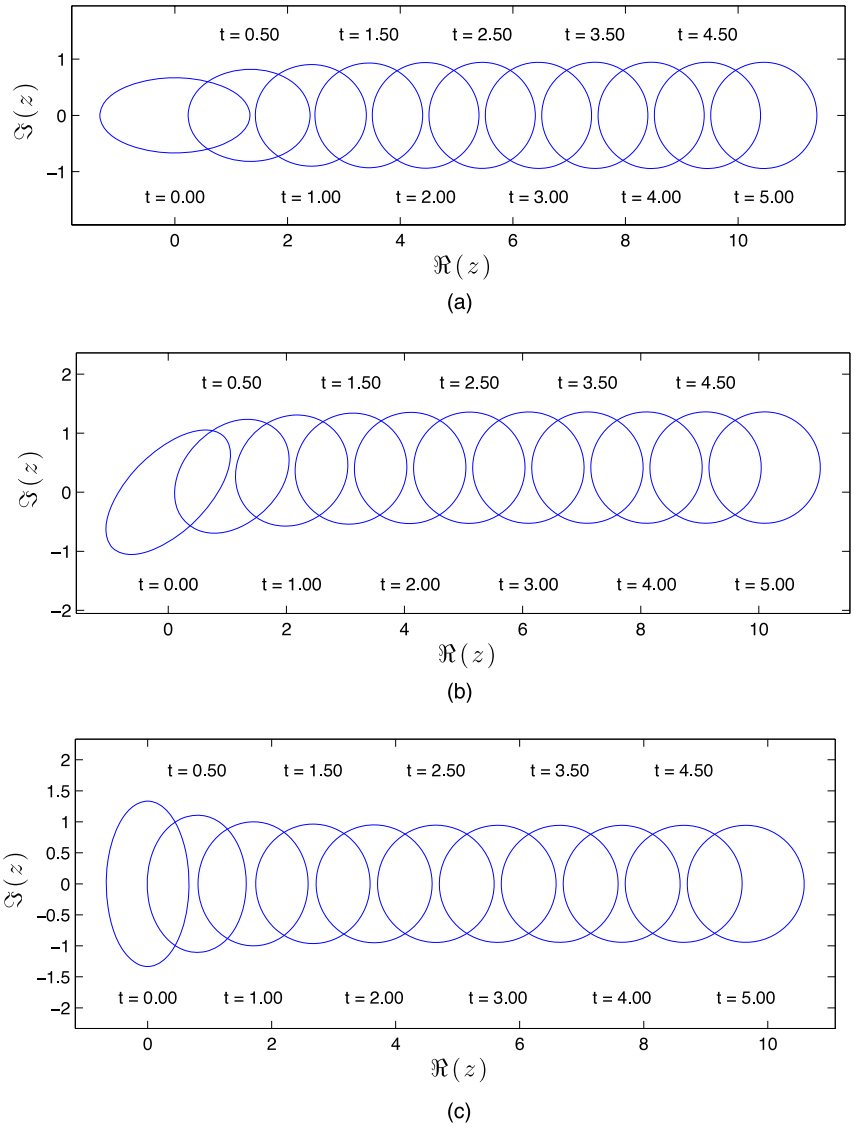

FIG. 3. Evolution of initially elliptical bubbles with semi-major axis inclined at three different angles θ_e to the positive real axis. In each case, the interface evolves into a circle. The initial interface is given by (4) with $a = 1$, $b = 1/3$, and $C = 0$. The results presented are for $N = 400$, $\Delta t = 0.001$, and $V = 1$. The corresponding times of the interface are displayed below and above the snapshots. (a) $\theta_e = 0$; (b) $\theta_e = \frac{\pi}{4}$; (c) $\theta_e = \frac{\pi}{2}$.

B. Initial interface leading to bubble breakup

Here, we consider bubbles with "simple" but non-elliptical initial fluid-bubble interfaces in uniform background flow and show how the initial geometry of the bubble may predict breakup by considering singularities of the Schwarz function of the initial interface.

Recall, the evolution of the interface can be expressed in complex form by the Schwarz function Eq. (3). It is well known (as demonstrated later in this section) that (3) implies singularities of the Schwarz function of the initial map remain fixed in the fluid domain and that these cannot cross the boundary of the bubble. This will lead to bubble deformation as the singular points are approached. This is investigated numerically.

Consider a bubble in a uniform flow with initial interface given by the rational map

$$z = \frac{a_0 + a_1\zeta + a_2\zeta^2}{\zeta + b_0}, \tag{37}$$

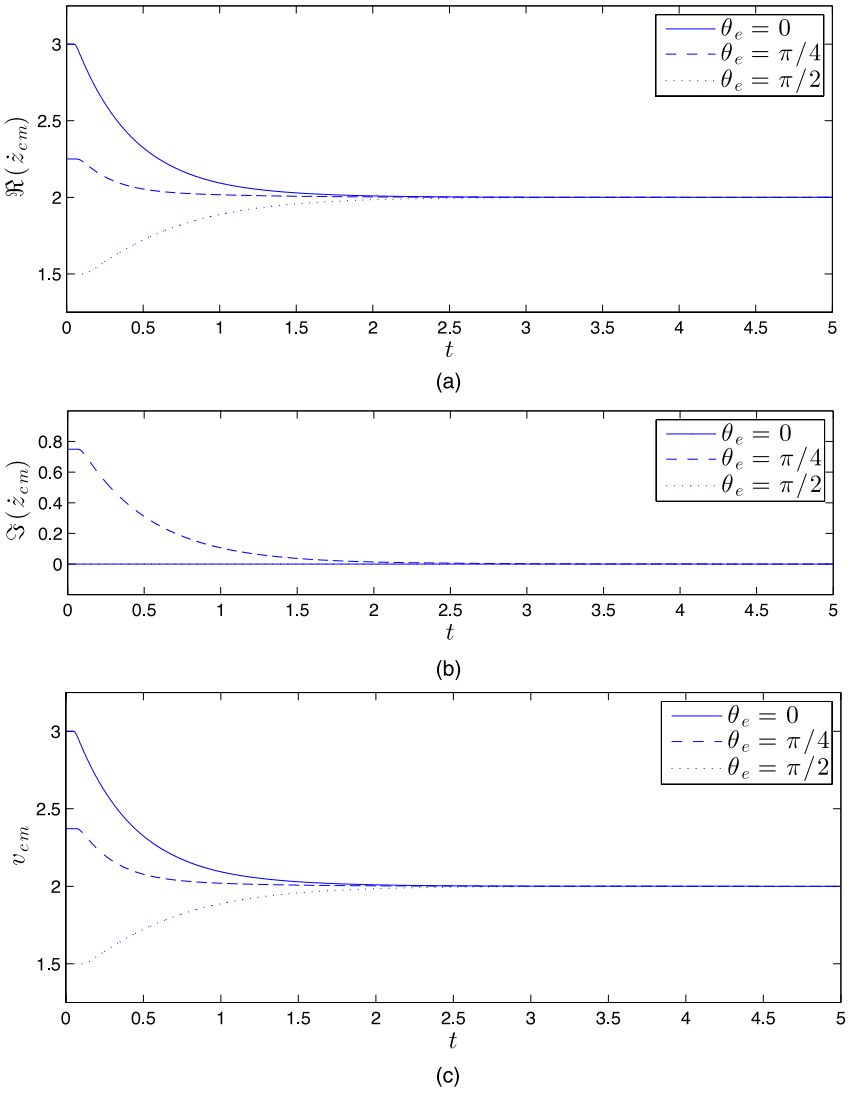

FIG. 4. Velocity of the centre of mass in the (a) real and (b) imaginary directions of the numerical solutions presented in Fig. 3 for the different elevation angles, θ_e, of elliptical bubbles. In (c), the overall speed v_{cm} is displayed.

which for particular parameters a_i and b_i, $i = 0, 1, 2$, gives a univalent map from D to the exterior of a crescent shaped bubble. Here, we will take a_i, b_i, to be real valued so that the bubble is symmetric about $\Re(z)$. For simplicity, we fix the coefficients $a_0 = -0.375$, $a_1 = -0.15$, $a_2 = 0.25$, and vary b_0 in order to generate different initial shapes. It is required that $|b_0| < 1$ for univalency. Map (37) has a singularity at $\zeta = -b_0$, which is mapped to infinity in the z-plane.

Since $\overline{\zeta}\zeta = 1$ on ∂D, the Schwarz function of the interface, $\partial\Omega(0)$, is given by

$$\mathcal{S} = \frac{a_0\zeta^2 + a_1\zeta + a_2}{\zeta + b_0\zeta^2}. \tag{38}$$

Function (38) has two singularities. Here, the only relevant singularity is at $\zeta = 0$ since it is the only one that lies inside D, i.e., it is mapped to the fluid domain as displayed in Fig. 7. Note that this singular point is downstream of the initial bubble position in the z-plane.

As $\zeta \to 0$, the map (37) gives

$$z = \frac{a_0}{b_0}\left(1 + \left[\frac{a_1}{a_0} - \frac{1}{b_0}\right]\zeta\right) + O(\zeta^2), \tag{39}$$

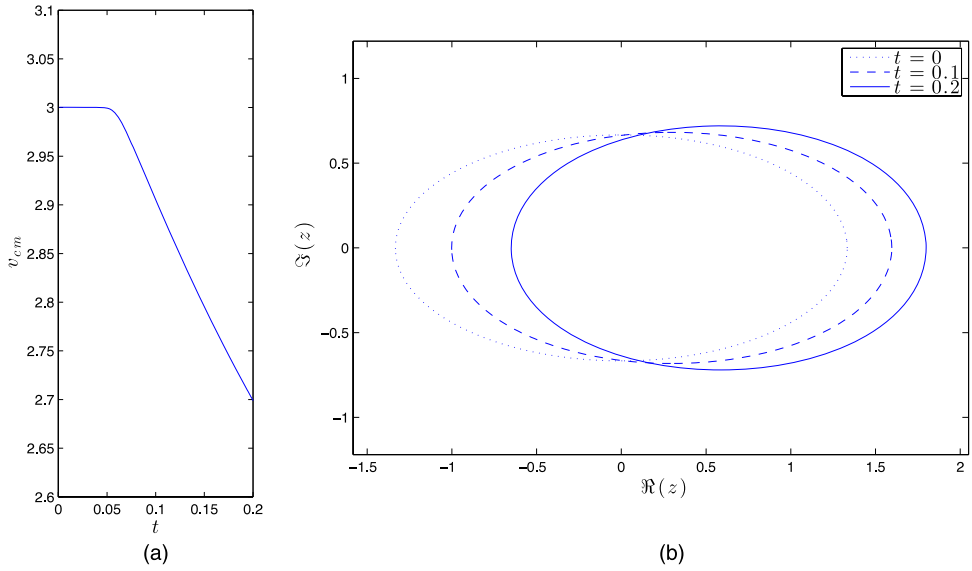

FIG. 5. Small time evolution of an initially elliptical bubble. The initial interface is given by (4) with $a = 1$, $b = 1/3$, $C = 0$, and with $\theta_e = 0$. The results presented are for $N = 400$, $\Delta t = 0.001$, and $V = 1$. Evolution of the speed of the centre of mass of the bubble is shown in (a) with snapshots of the bubble interface shown in (b).

hence, expanding $\mathcal{S}$ to leading order yields

$$\begin{aligned}\mathcal{S} &= \frac{a_2}{\zeta} + (a_1 - a_2 b_0) + O(\zeta) \\ &= \frac{a_0 a_2}{b_0}\left(\frac{a_1}{a_0} - \frac{1}{b_0}\right)\frac{1}{(z - a_0/b_0)} + (a_1 - a_2 b_0) + O(z - a_0/b_0).\end{aligned} \tag{40}$$

It is clear that the Schwarz function has a singularity at the point $z_0 = a_0/b_0 = z(0)$, as expected. Differentiating (40) with respect to time gives

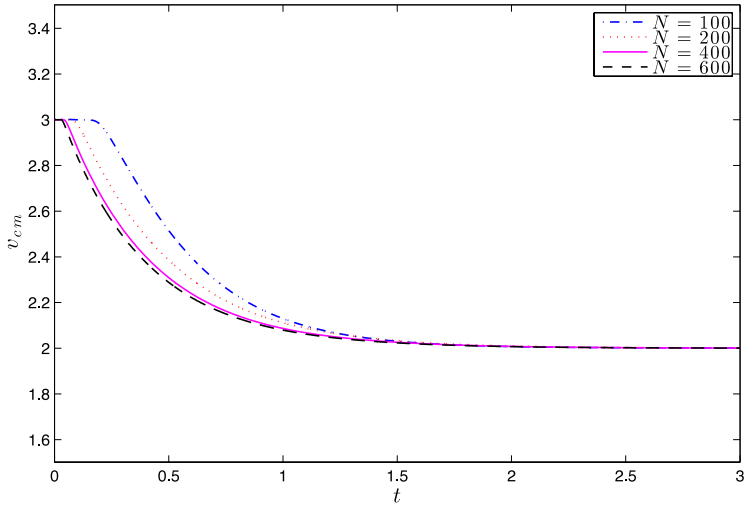

FIG. 6. Effect of increasing the number of mesh points, N, on v_{cm} of an initially elliptical bubble as the interface evolves to the stable circular bubble travelling with speed $U = 2V$. The initial bubble is given by (4) with $a = 1$, $b = 1/3$, $C = 0$, and $\theta_e = 0$. For the results presented, $\Delta t = 0.001$ and the background flow has speed $V = 1$.

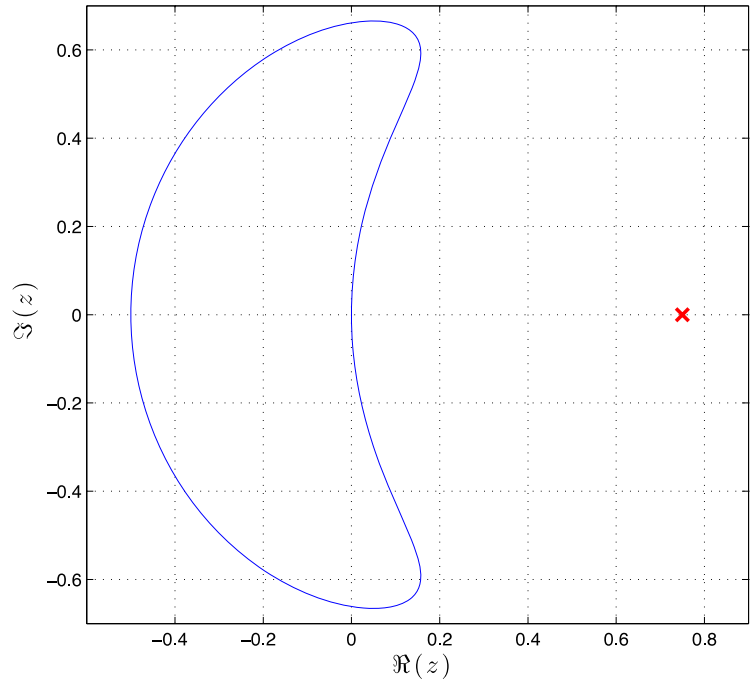

FIG. 7. Initial bubble shape given by (37), and location of the Schwarz function singularity (38) with $a_0 = -0.375$, $a_1 = 0$, $a_1 = -0.15$, $a_2 = 0.25$, and $b_0 = -0.5$. The singularity is marked by a cross and is mapped from the interior of D to the initial fluid domain, $\Omega(0)$.

$$\frac{\partial \mathcal{S}}{\partial t} = \left(\frac{a_0 a_2}{b_0}\left[\frac{a_1}{a_0} - \frac{1}{b_0}\right]\right)\frac{d}{dt}\left(\frac{a_0}{b_0}\right)\frac{1}{(z-z_0)^2} + \frac{d}{dt}\left(\frac{a_0 a_2}{b_0}\left[\frac{a_1}{a_0} - \frac{1}{b_0}\right]\right)\frac{1}{(z-z_0)} + \frac{d}{dt}(a_1 - a_2 b_0) + O(z-z_0), \quad (41)$$

i.e., $\dot{\mathcal{S}}$ has singularities at z_0 of first and second order due to the initial shape describing the interface of the bubble. Since the background flow is a steady uniform flow (no sources, sinks, or dipoles), $\partial_z w$ is analytic in $\Omega(t)$, and since (3) holds away from $\partial\Omega(t)$, (41) implies $d\left((a_1 a_2/b_0) - (a_0 a_2/b_0^2)\right)/dt = 0$ and $d(a_0/b_0)/dt = 0$. The latter implies $\dot{z}_0 = 0$, i.e., z_0 is constant, and so the singularity of $\mathcal{S}$ remains stationary. Since this point must always lie in the fluid domain, the bubble boundary cannot cross z_0. That is, the interface will evolve such that z_0 is avoided.

Fig. 8 shows the evolution of initial crescent shaped bubbles given by map (37) for various values of b_0, where the background flow has speed $V = 1$. In all cases, the front and rear of the bubble interface become progressively close until they collide after which it is expected that the bubble will "split" symmetrically. We do not extend the numerical solutions beyond this time. As the front of the initial bubble becomes less convex with respect to the interior of the bubble (and direction of the flow), the bubble splits at more than one location, as can be seen in Fig. 8(e). Furthermore, as the front of the initial bubble shape changes from convex to concave, the numerical results suggest the bubble no longer splits, as is the case of Fig. 9 where $b_0 = -0.1$. In the same limit of (40), the singularity of $\mathcal{S}$ is located further away from the starting location of the bubble. Instead of splitting, the bubble evolves to a circle, similar to the behaviour of the elliptical bubble observed in Sec. IV B (which have Schwarz function singularities at infinity). That is, in Fig. 9, the interface passes over the location of the singularity of the Schwarz function from the initial interface. Mathematically, this is not permitted but it may be explained because of numerical instabilities which force the solution rapidly to a circular interface and that numerical effects (e.g., instabilities and filtering) cause information on the initial Schwarz function singularity to be lost. The larger the distance the bubble has to travel before encountering the Schwarz function singularity the greater these numerical effects are.

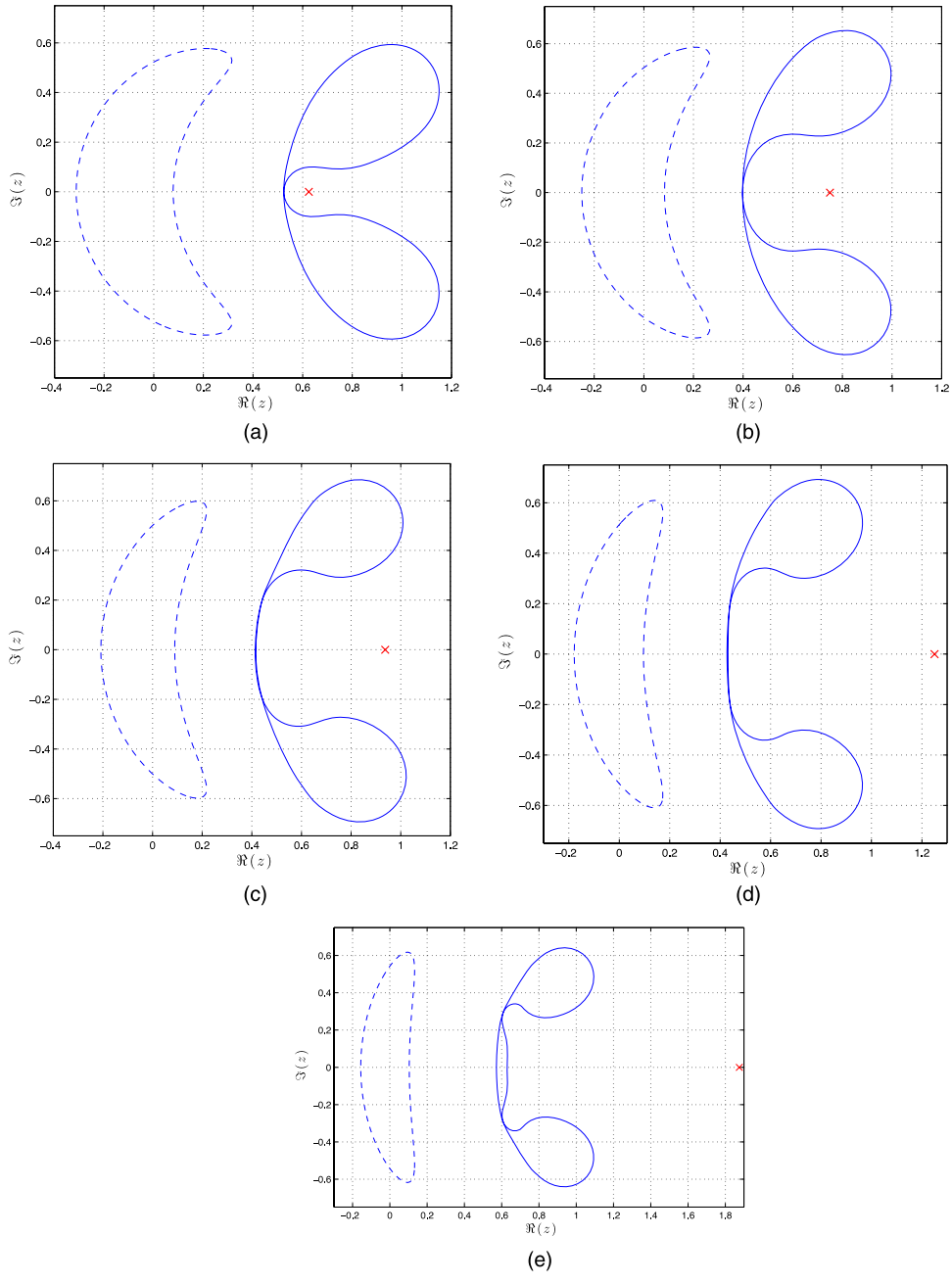

FIG. 8. Snapshots of the bubble interface at the initial time $t = 0$ (dashed) and when the interface collides with itself at time $t = t_e$ (solid). Here, the results presented are for $N = 400$, $\Delta t = 0.0005$, and $V = 1$. (a) $b_0 = -0.6$, $t_e = 0.4875$; (b) $b_0 = -0.5$, $t_e = 0.405$; (c) $b_0 = -0.4$, $t_e = 0.43$; (d) $b_0 = -0.3$, $t_e = 0.43$; (e) $b_0 = -0.2$, $t_e = 0.555$.

Now consider an initially crescent shaped bubble which is asymmetric in $\Re(z)$. Fig. 10 shows the evolution of a bubble with initial interface given by (37) rotated through an angle $\theta = -\pi/4$ (i.e., we replace z by $e^{-i\theta}z$) with $b_0 = -0.8$. Although the singularity of the corresponding Schwarz function of the initial interface lies directly downstream of a portion of the bubble, it can be seen that the bubble evolves to the circular solution in a manner so as to avoid contact with the singularity z_0. If the angle of rotation is reduced to $\theta = -\pi/8$, as in Fig. 11, the bubble will split asymmetrically before the interface reaches z_0.

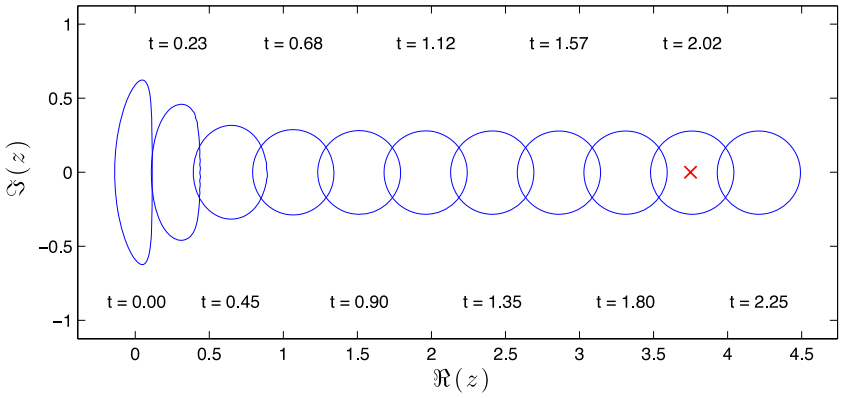

FIG. 9. Evolution of an initially crescent shaped bubble given by map (37) with $b_0 = -0.1$ and corresponding Schwarz function singularity in $\Omega(0)$ is marked by a cross. The results presented are for $N = 400$, $\Delta t = 0.0005$, and $V = 1$. The corresponding times of the interface are displayed below and above the snapshots.

It is possible to use (37) to find an exact solution for the evolution of a Hele-Shaw bubble. The four unknown parameters a_0, a_1, a_2, and b_0 are governed by four ODEs, two of which come from (41); namely, that the strength and location of the singularity of the Schwarz function at $z = z_0$ are constant. A further two independent ODEs can be derived by considering the behaviour of the Schwarz function (38) as $z \to \infty$ and applying (3) with $\partial_z w \to V + O(z^{-2})$ in the same limit. Equating terms of $O(1)$ and $O(z^{-1})$ yields the additional two ODEs, the latter of which is equivalent to bubble area conservation (see also Sec. V for a similar derivation). These ODEs can then be integrated numerically to find a_0, a_1, a_2, and b_0 given their initial values. This has, in fact, been done and the results (not shown) differ from those in Figs. 8–10: while they confirm that the Schwarz function singularity plays an important role in the bubble evolution in that they are avoided by the bubble boundary, cusps form and the solution breaks down in finite time. It is evident that the present numerical procedure provides sufficient smoothing to prevent such cusps forming and that instead breakdown here occurs via bubble breakup.

C. Finite blob pinch off within a bubble

Here, we present numerical results showing a different type of change in bubble topology. Consider the map given by

$$z = \frac{\alpha_0 + \alpha_1 \zeta}{(\zeta + \beta_1)(\zeta + \beta_2)}, \tag{42}$$

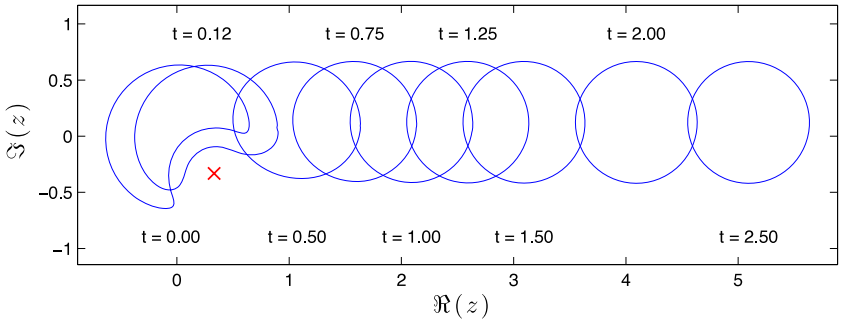

FIG. 10. Evolution of an initially crescent shaped bubble given by map (37) with $b_0 = -0.8$ rotated by angle $\theta_e = -\pi/4$. The results presented are for $N = 400$, $\Delta t = 0.0005$, and $V = 1$. The corresponding times of the interface are displayed below and above the snapshots. The Schwarz function singularity in $\Omega(0)$ is marked by a cross.

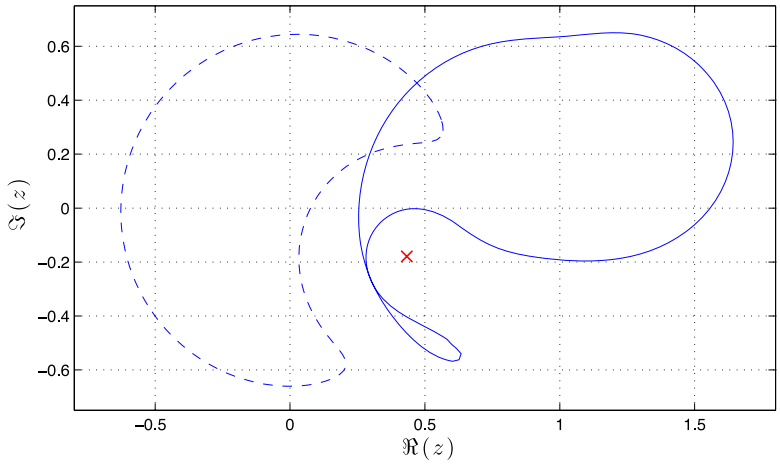

FIG. 11. Snapshot of the bubble interface at $t = 0$ (dashed) and $t = 0.445$ (solid), where the initial interface is given by map (37) with $b_0 = -0.8$, rotated by angle $\theta_e = -\pi/8$. The corresponding Schwarz function singularity in $\Omega(0)$ is marked by a cross. The results presented are for $N = 400$, $\Delta t = 0.0005$, and $V = 1$.

giving a crescent shape shown by the dashed line in Fig. 12(a). The coefficients α_i, β_i, $i = 0, 1, 2$, are real and such that (42) maps D to the exterior of the bubble. Here, the map has a singular point lying inside D, namely, $\zeta = -\beta_1$ where $-1 < \beta_1 < 1$ so that the map remains univalent on D, and one singular point outside D at $\zeta = -\beta_2$, i.e., $|\beta_2| > 1$.

The Schwarz function of $\partial\Omega(t)$ in this case is given by

$$\mathcal{S} = \frac{\alpha_0\zeta + \alpha_1}{(1 + \beta_1\zeta)(1 + \beta_2\zeta)}, \tag{43}$$

which gives one singularity for $\mathcal{S}$ in the fluid domain at position $z(-1/\beta_2)$ lying on the real axis, downstream of the initial bubble, shown in Fig. 12(a) for $t = 0$, marked by a cross. Again, we denote this point by z_0, and by a similar argument presented in Sec. IV C, z_0 can be shown to be constant.

Fig. 12 shows the evolution of a bubble with initial interface given by (42) with $\alpha_0 = \alpha_1 = -0.25$, $\beta_1 = -0.3$, and $\beta_2 = 1.15$ subject to a background uniform flow of unit speed, i.e., $V = 1$. As the bubble translates downstream, the "horns" of the crescent become smoother and begin to close at the front of the bubble. Subsequently, a region of fluid is trapped by the engulfing bubble and the interface of the bubble collides with itself, beyond which it is expected the trapped fluid blob pinches off and the bubble forms a ring around the interior, disconnected fluid blob. The interior blob is centred on the Schwarz functions' singularity, $z_0 = z(-1/\beta_2)$—see Fig. 12(b). Since the pressure in the bubble region remains constant, the blob inside the bubble is expected to remain stationary once pinched off as no information of the background flow reaches its interface, whilst the outer interface is expected to translate downstream until the interior blob collides with the rear of the bubble, eventually reattaching with the main body of fluid. As $t \to \infty$, we speculate that the bubble attracts to the aforementioned circular solution, travelling at speed twice the background flow.

V. STABILITY OF ELLIPTICAL BUBBLES

As noted in Sec. I, Vasconcelos and Mineev-Weinstein[12] have given a stability analysis for time-dependent solutions (which survive for all time) describing bubbles in finite width channels. They show that the bubble with speed $U = 2V$ is the only stable attractor for these solutions. In the small bubble limit, in which the bubble is far from the channel walls, this corresponds to a circular bubble (in an unbounded Hele-Shaw cell). In this section, an alternative stability analysis is given in which an elliptical bubble is shown to be unstable to a particular type of perturbation (this being sufficient to guarantee that it is unstable) and that it evolves toward a circle.

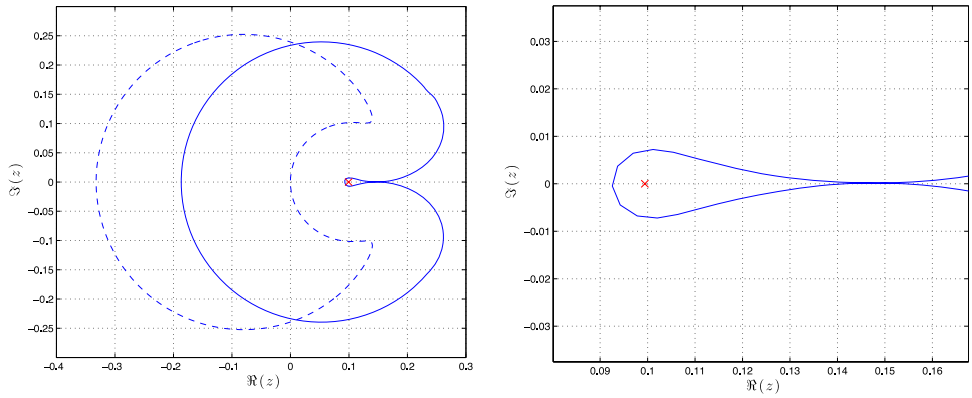

FIG. 12. Snapshot of bubble interface at $t = 0$ (dashed) and $t = 0.066\,25$ (solid), where the initial interface is given by map (42) with $\alpha_0 = -1$, $\alpha_1 = -1$, $\beta_1 = -0.3$, and $\beta_2 = 1.15$. The corresponding Schwarz function singularity in $\Omega(0)$ is marked by a cross. Close-up of the blob pinched off by the surrounding bubble is shown in (b). Results are presented for $N = 400$, $\Delta t = 0.000\,25$, and $V = 1$.

Consider the stability of the steady translating elliptical bubble solutions to a certain class of perturbations having the form

$$z = c + a\zeta + \frac{b}{\zeta - \epsilon}, \tag{44}$$

where, now, the *exterior* of the unit ζ-disc is mapped to the exterior of the perturbed elliptical bubble (i.e., the flow domain $\Omega(t)$), and the time-varying parameters are such that ϵ is small, $a \neq 0$, b and c are real. If $\epsilon \equiv 0$, note that (44) is the map describing an elliptical bubble. The Schwarz function of the interface is given by

$$\mathcal{S} = c + \frac{a}{\zeta} - \frac{b}{\epsilon} + \frac{b}{\epsilon}\frac{1}{1 - \epsilon\zeta}. \tag{45}$$

In the limit $z \to \infty$, it can be shown from (44) and (45) that

$$\mathcal{S} = c - \frac{b}{\epsilon} + \frac{1}{z}\left(a^2 - \frac{ab}{\epsilon^2}\right) + O(z^{-2}). \tag{46}$$

Applying the Schwarz function equation (3), as $z \to \infty$, yields

$$\frac{d}{dt}\left(c - \frac{b}{\epsilon}\right) + \frac{d}{dt}\left(a^2 - \frac{ab}{\epsilon^2}\right)\frac{1}{z} + O(z^{-2}) = 2V. \tag{47}$$

The equality of the above equation gives at $O(1)$ and $O(z^{-1})$

$$\frac{d}{dt}\left(c - \frac{b}{\epsilon}\right) = 2V, \tag{48a}$$

$$\frac{d}{dt}\left(a^2 - \frac{ab}{\epsilon^2}\right) = 0. \tag{48b}$$

Now, $\mathcal{S}$ has a singularity lying at $\zeta = 1/\epsilon$ exterior to the unit ζ-circle (i.e., in the pre-image fluid domain), about which the Schwarz function has leading order behaviour as $z \to z_0$ of the form

$$\mathcal{S} = -\left(\frac{ab}{\epsilon^2} - \frac{b^2}{(1-\epsilon^2)^2}\right)\frac{1}{(z - z_0)} + c + a\epsilon - \frac{b}{\epsilon} - \frac{b^2\epsilon}{a(1-\epsilon^2)^3 - b\epsilon^2(1-\epsilon^2)} + O(z - z_0), \tag{49}$$

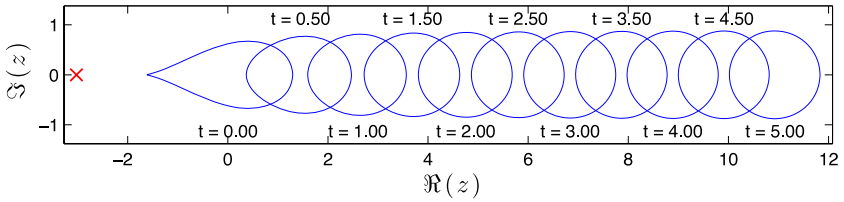

FIG. 13. Evolution of an initially perturbed elliptical bubble given by map (44) with $c(0) = 0$, $a(0) = 1$, $b(0) = 1/3$, and $\epsilon = -0.3803$ and the background flow with speed $V = 1$. The cross denotes the location of the Schwarz function singularity of the initial interface. The corresponding times of the interface are displayed below and above the snapshots.

where $z_0 = z(\epsilon^{-1}) = c + a/\epsilon + b\epsilon/(1-\epsilon^2)$. Differentiating with respect to time yields

$$\frac{\partial \mathcal{S}}{\partial t} = -\frac{dz_0}{dt}\left(\frac{ab}{\epsilon^2} - \frac{b^2}{(1-\epsilon^2)^2}\right)\frac{1}{(z-z_0)^2} - \frac{d}{dt}\left(\frac{ab}{\epsilon^2} - \frac{b^2}{(1-\epsilon^2)^2}\right)\frac{1}{(z-z_0)} + \frac{d}{dt}\left(c + a\epsilon - \frac{b}{\epsilon} - \frac{b^2\epsilon}{a(1-\epsilon^2)^3 - b\epsilon^2(1-\epsilon^2)}\right) + O(z-z_0). \quad (50)$$

Since the velocity potential must be analytic in the fluid domain $\Omega(t)$, i.e., there exist no hydrodynamic singularities in the flow, and since the Schwarz function equation, $\dot{\mathcal{S}} = 2\partial_z w$, must hold over the fluid domain, then as $\zeta \to 1/\epsilon$

$$\frac{d}{dt}\left(\frac{ab}{\epsilon^2} - \frac{b^2}{(1-\epsilon^2)^2}\right) = 0, \quad (51a)$$

$$\frac{d}{dt}\left(c + \frac{a}{\epsilon} + \frac{b\epsilon}{1-\epsilon^2}\right) = 0. \quad (51b)$$

Along with the above equations, the area of the bubble must also be conserved. The area can be calculated using Green's theorem, with integration around the unit ζ-circle to yield

$$A = \frac{1}{2i}\oint_{\partial D} \overline{z} z_\zeta d\zeta = \pi\left(a^2 - \frac{b^2}{(1-\epsilon^2)^2}\right). \quad (52)$$

Note that (51a) is a linear combination of (48b) and (52) and, so, provides no new information on the evolution of the parameters ϵ, a, b, and c. Therefore, there are four equations, namely, (48a), (48b), (51b), and (52) governing the evolution of map (44) for the perturbed ellipse.

In the case of $\Im(\epsilon) \neq 0$, b is no longer real in general, and the set of equations governing the evolution of the time dependent parametric map (44) are

$$\frac{d}{dt}\left(\overline{c} - \frac{\overline{b}}{\overline{\epsilon}}\right) = 2V, \quad (53a)$$

$$\frac{d}{dt}\left(a^2 - \frac{a\overline{b}}{\overline{\epsilon}^2}\right) = 0, \quad (53b)$$

$$\frac{d}{dt}\left(c + \frac{a}{\overline{\epsilon}} + \frac{b\overline{\epsilon}}{1-|\epsilon|^2}\right) = 0, \quad (53c)$$

$$a^2 - \frac{|b|^2}{(1-|\epsilon|^2)^2} = \frac{A}{\pi}. \quad (53d)$$

Again, there exists an extra equation corresponding to (51a), namely,

$$\frac{d}{dt}\left(\frac{a\overline{b}}{\overline{\epsilon}^2} - \frac{|b|^2}{(1-|\epsilon|^2)^2}\right) = 0. \quad (54)$$

It can be seen that (54) is a linear combination of (53b) and (53d). Therefore, (53) gives a set of three complex equations and one real equation for the complex parameters c, b, and ϵ,

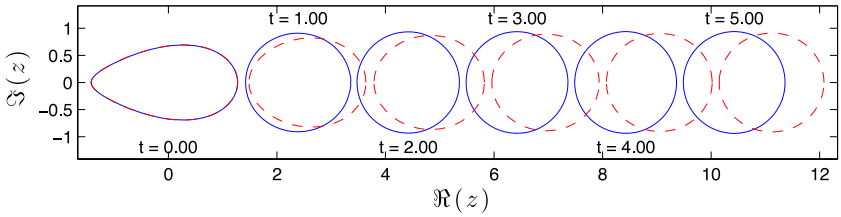

FIG. 14. Evolution of an initially perturbed elliptical bubble given by (44) with $c(0) = 0$, $a(0) = 1$, $b(0) = 1/3$, and $\epsilon(0) = -0.2113$. Comparison between numerical simulation (solid) and solution to the set of equations (53) (dashed) is shown at multiple snapshots. The corresponding times are displayed below and above the interface snapshot pairs. Numerical results (solid) are presented for $N = 200$ and $\Delta t = 0.001$. The background flow speed is set to $V = 1$.

and the real parameter a. Now, as the bubble travels in the positive $\Re(z)$ direction, as $t \to \infty$, $c \to \infty$. From (53c), $\overline{\epsilon} \to 0$ as $t \to \infty$ to balance c terms. The alternative possibility of a and $b \to \infty$ can be ruled out by virtue of (53b) and (53d). Equation (53b) in turn implies that $\overline{b} \to 0$ and hence (53d) implies $a \to$ constant as $t \to \infty$. Using (53a) and (53c) further implies that $\overline{\epsilon} \to -a/\left(\overline{c} + \left[b\overline{\epsilon}/(1 - |\epsilon|^2)\right] - K\right) \sim -a/t$, where K is constant, i.e., ϵ approaches zero from below. Equation (53b) implies that $b \sim \epsilon^2$ as $t \to \infty$, that is, b must approach zero at least as t^{-2} as $t \to \infty$. Finally, (53a) implies $c \to 2Vt$ as $t \to \infty$. Thus, the bubble becomes circular, travelling at speed twice the background flow.

Fig. 13 shows the evolution of an initially elliptical, perturbed bubble given by map (44) where the time dependent coefficients are found by solving the nonlinear set of coupled equations (53a)–(53d), numerically.

The numerical simulations in Sec. IV A demonstrate the evolution of an initially elliptical bubble to a circular bubble where the transition of shape takes place over a short distance, no more than 2–3 semi-major axis lengths of the initial bubble shape. That is, an otherwise steady shape solutions evolves to the circular bubble due to the numerical instabilities, which are implicit at each time step of the numerical algorithm (cf. Sec. III C). The rapid evolution towards the steadily translating circular bubble, as soon as the numerical instability perturb the interface, can be seen in Fig. 6. Therefore, with the added effects of numerical instability, it is expected that numerical simulations with initial bubble interface given by (44) would exhibit an enhanced rate of evolution to the circular bubble as compared with evolution governed by the set of coupled equations given in (53). Figure 14 shows a comparison between numerical results and evolution governed by the set of equations (53). It is observed that the numerical simulation evolves to the circular bubble more quickly, as expected. However, it is important to emphasise that in both cases, the dynamics of the interface are such that the bubble perimeter becomes circular, i.e., the parameters b and ϵ of (44) decay to zero as $t \to \infty$.

VI. CONCLUSIONS

A boundary integral formulation and numerical method for the study of Hele-Shaw bubble evolution in an unbounded cell is presented in Sec. III A by considering the decomposition of the velocity potential into the background flow plus a "local" solenoidal part.

In Sec. IV A, the numerical results demonstrate that for initially elliptical bubbles, the only (attractive) solution as $t \to \infty$ is a circular bubble travelling at a steady speed of twice the background flow V. Since surface tension effects are not included, the results are related to the analytical results of Vasconcelos and Mineev-Weinstein[12] for the selection problem in a channel geometry, where it is shown that the selected bubble also propagates with speed $2V$. A stability argument in Sec. V based on a perturbed ellipse provides further evidence the circular bubble with speed $U = 2V$ as being the stable attractor. However, it should be noted that the filtering method has a smoothing effect akin to surface tension. Thus, it is not clear if the numerical results support the ZST selection mechanism, or if the selection is a result of the filtering mechanism itself.

In Secs. IV B and IV C, it is shown for some initial shapes of $\partial\Omega(0)$, it is possible that the evolution of $\partial\Omega(t)$ results in one of two types of topological change. In the former, the numerical results suggest the bubble may split, becoming multiply connected. In the latter, the bubble encloses a region of viscous fluid, i.e., a singly connected viscous fluid domain eventually becomes two disconnected regions. The numerical results suggest the singularities of the Schwarz function of the initial interface play an important role on the evolution of the interface, since mathematically the boundary cannot cross the singularity.

ACKNOWLEDGMENTS

A.H.K. would like to thank the Department of Mathematics, University College London for providing funding for research via the Departmental Teaching Assistantship programme. Valuable discussions with Professor G. L. Vasconcelos are gratefully acknowledged. The authors would also like to thank Dr. M. C. Dallaston for useful discussions.

[1] B. Gustafsson and A. Vasil'ev, *Conformal and Potential Analysis in Hele-Shaw Cells*, Advances in Mathematical Fluid Mechanics (Birkhäuser Verlag, Basel, 2006).
[2] M. Mineev-Weinstein and A. Zabrodin, "Whittam-Toda hierarchy in the Laplacian growth problem," J. Nonlinear Math. Phys. **8**, 212–218 (2001).
[3] M. Mineev-Weinstein, M. Putinar, and R. Teodorescu, "Random matrices in 2D, Laplacian growth and operator theory," J. Phys. A: Math. Theor. **41**, 1–74 (2008).
[4] P. Y. Polubarinova-Kochina, "On the motion of the oil contour," Dokl. Akad. Nauk SSSR **47**, 254–257 (1945).
[5] L. A. Galin, "Unsteady filtration with a free surface," Dokl. Akad. Nauk SSSR **47**, 246–249 (1945).
[6] P. G. Saffman and G. I. Taylor, "The penetration of a fluid into a porous medium or Hele-Shaw cell containing a more viscous liquid," Proc. R. Soc. London, Ser. A **245**, 312–320 (1958).
[7] G. I. Taylor and P. G. Saffman, "A note on the motion of bubbles in a Hele-Shaw cell and porous medium," Q. J. Mech. Appl. Math. **12**, 267–279 (1959).
[8] J. M. Vanden-Broeck, "Fingers in a Hele-Shaw cell with surface tension," Phys. Fluids **26**, 2033–2034 (1983).
[9] S. Tanveer, "Analytic theory for the selection of a symmetric Saffman-Taylor finger in a Hele-Shaw cell," Phys. Fluids **30**, 1589–1605 (1987).
[10] D. A. Kessler and H. Levine, "Microscopic selection of fluid fingering patterns," Phys. Rev. Lett. **86**, 4532–4535 (2001).
[11] M. Mineev-Weinstein, "Selection of the Saffman-Taylor finger width in the absence of surface tension: An exact result," Phys. Rev. Lett. **80**, 2113–2116 (1998).
[12] G. L. Vasconcelos and M. Mineev-Weinstein, "Selection of the Taylor-Saffman bubble does not require surface tension," Phys. Rev. E **89**, 1–5 (2014).
[13] A. Sarkissian and H. Levine, "Comment on 'Selection of the Saffman-Taylor finger width in the absence of surface tension: An exact result,"' Phys. Rev. Lett. **81**, 4528 (1998).
[14] M. Mineev-Weinstein, "Mineev-Weinstein replies," Phys. Rev. Lett. **81**, 4529 (1998).
[15] J. Casademunt and F. X. Magdaleno, "Comment on 'Selection of the Saffman-Taylor finger width in the absence of surface tension: An exact result,"' Phys. Rev. Lett. **81**, 5950 (1998).
[16] R. F. Almgren, "Comment on "Selection of the Saffman-Taylor finger width in the absence of surface tension: An exact result,"" Phys. Rev. Lett. **81**, 5951 (1998).
[17] M. Mineev-Weinstein, "Mineev-Weinstein replies," Phys. Rev. Lett. **81**, 5952 (1998).
[18] M. Siegel, S. Tanveer, and W. Dai, "Singular effects of surface tension in evolving Hele-Shaw flows," J. Fluid Mech. **323**, 201–236 (1996).
[19] S. Tanveer, "Surprises in viscous fingering," J. Fluid Mech. **409**, 273–308 (2000).
[20] E. Alvarez-Lacalle, J. Casademunt, and J. Eggers, "Pinch-off singularities in rotating Hele-Shaw flows at high viscosity contrast," Phys. Rev. E **80**, 1–10 (2009).
[21] S. Y. Lee, E. Bettelheim, and P. Wiegmann, "Bubble break-off in Hele-Shaw flows: Singularities and integrable structures," Physica D **219**, 23–34 (2006).
[22] D. Crowdy, "Circulation-induced shape deformations of drops and bubbles: Exact two-dimensional models," Phys. Fluids **11**, 2836–2845 (1999).
[23] V. Entov and P. Etingof, "On the breakup of air bubbles in a Hele-Shaw cell," Eur. J. Appl. Math. **22**, 125–149 (2011).
[24] T. Maxworthy, "Bubble formation, motion and interaction in a Hele-Shaw cell," J. Fluid Mech. **173**, 95–114 (1986).
[25] J. W. McLean and P. G. Saffman, "The effect of surface tension on the shape of fingers in a Hele-Shaw cell," J. Fluid Mech. **102**, 455–469 (1981).
[26] E. D. Kelly and E. J. Hinch, "Numerical solution of Hele-Shaw flows driven by a quadrupole," Eur. J. Appl. Math. **8**, 551–566 (1997).
[27] M. Dallaston and S. McCue, "Numerical solution to the Saffman-Taylor finger problem with kinetic undercooling regularisation," ANZIAM J. **52**, 124–138 (2011), available at http://journal.austms.org.au/ojs/index.php/ANZIAMJ/article/view/3924.
[28] T. Y. Hou, J. S. Lowengrub, and M. J. Shelley, "Removing the stiffness from interfacial flows with surface tension," J. Comput. Phys. **114**, 312–338 (1994).
[29] G. Tryggvason and H. Aref, "Numerical experiments on Hele-Shaw flow with a sharp interface," J. Fluid Mech. **136**, 1–30 (1983).

[30] H. D. Ceniceros, T. Y. Hou, and H. Si, "Numerical study of Hele-Shaw flow with suction," Phys. Fluids **11**, 2471–2486 (1999).
[31] S. D. Howison, "Complex variable methods in Hele-Shaw moving boundary problems," Eur. J. Appl. Math. **3**, 209–224 (1992).
[32] N. R. McDonald, "Generalised Hele-Shaw flow: A Schwarz function approach," Eur. J. Appl. Math. **22**, 517–532 (2011).
[33] A. H. Khalid, N. R. McDonald, and J. M. Vanden-Broeck, "Hele-Shaw flow driven by an electric field," Eur. J. Appl. Math. **25**, 425–447 (2014).
[34] S. Tanveer, "New solutions for steady bubbles in a Hele-Shaw cell," Phys. Fluids **30**, 651–658 (1987).
[35] F. R. Tian and G. L. Vasconcelos, "Rotation invariance for steady Hele-Shaw flows," Phys. Fluids A **5**, 1863–1865 (1993).
[36] J. M. Vanden-Broeck, "Steep solitary waves in water of finite depth with constant vorticity," J. Fluid Mech. **274**, 339–348 (1994).
[37] G. R. Baker, "A test of the method of Fink & Soh for following vortex-sheet motion," J. Fluid Mech. **100**, 209–220 (1980).
[38] M. S. Longuet-Higgins and E. D. Cokelet, "The deformation of steep surface waves on water. I. A numerical method of computation," Proc. R. Soc. London, Ser. A **350**, 1–26 (1976).
[39] J. M. Aitchison and S. D. Howison, "Computation of Hele-Shaw flows with free boundaries," J. Comput. Phys. **60**, 376–390 (1985).
[40] R. Krasny, "A study of singularity formation in a vortex sheet by the point-vortex approximation," J. Fluid Mech. **167**, 65–93 (1986).
[41] D. L. Phillips, "A technique for the numerical solution of certain integral equations of the first kind," J. ACM. **9**, 84–97 (1962).
[42] S. Twomey, "On the numerical solution of Fredholm integral equations of the first kind by the inversion of the linear system produced by quadrature," J. ACM. **10**, 97–101 (1963).
[43] A. Tatulchenkov and A. Cebers, "Complex bubble dynamics in a vertical Hele-Shaw cell," Phys. Fluids **17**, 1–9 (2005).